Recovering Scenes by Polarization Analysis

Yoav Y. Schechner   and   Nir Karpel

Dept. of Electrical Engineering
Technion - Israel Inst. Technology
Haifa 32000, ISRAEL

`yoav@ee.technion.ac.il` , `karpeln@tx.technion.ac.il`

Abstract— We devise a computer vision approach which removes degradation effects in optical underwater imaging. It exploits natural illumination. By analysis of the physical effects of visibility degradation, we associate natural backscatter with partial polarization of light. This is contrary to prior studies which have associated polarization with light emanating from the objects, rather than the backscatter. Our algorithm takes advantage of this aspect to invert the image formation process. In this paper we show that our method achieves a much better visibility recovery, compared to prior methods. This is demonstrated in underwater experimentation in the sea. In addition, the physics-based analysis of the polarization filtered images recovers a range-map of the scene. This allows 3D rendering of the scene from various viewpoints.

I. Underwater Visibility Problems

Underwater visibility is typically very poor [6][13][16][19][33][40]. For this reason, a lot of research effort is being invested in acoustic imaging, which can penetrate water more easily. However, acoustics sensors have their own shortcomings: they have a much lower spatial resolution than optical systems [3][4][25]; sound waves may undergo convoluted and distorted paths in the water due to refraction between layers of water [17]; reverberations create false detections [35], while scattering by tiny particles having acoustic contrast creates speckle noise [17][24]; sonar detection is prone to noise coming from electronic sources and suffers from directionality problems associated with sidelobes of the acoustic antenna [39]. Acoustic sensors trade spatial resolution for detection range, since acoustic radiation is attenuated quickly in water as the acoustic frequency increases [17]. Low frequencies require systems that are very large [12][34], in order to obtain any spatial resolution. In addition, active sonar is disadvantageous in stealth tasks [3]. Finally, the visual interpretation of acoustic images is difficult, since we as humans have not evolved to view fields of acoustic reflectances.

To avoid these problems, there is need for underwater optical imaging systems. However, in addition to disrupting human interpretation of scenes, the poor underwater optical visibility hinders computer vision [10] tasks, e.g., those based on stereo triangulation or on structure from motion. It is important to alleviate these visibility problems, in order to enhance engineering applications [1][2][9][11][19][23][32][33][40], as well as research in marine biology [8][15][37][40] archaeology [6] and mapping [41].

We have recently introduced a physics-based approach for recovery of visibility when imaging underwater scenes in natural illumination [28]. It explicitly relies on the image formation process, and thus accounts for the complex spatially varying degradation effects which exist in submerged scenes. The approach relies on raw images taken through different states of a *polarizing filter*. We have shown that due to the polarization of natural backscatter (veiling light), these raw images have slight photometric differences. Thus, these differences serve as initial cues for an algorithm that factors out the effects that degrade underwater scenes.

In this paper we first give a brief overview of our method. Then, we concentrate on comparison of its results to ones obtained by prior methods. In particular, we show that the method is superior to other methods based on polarization, as well as to standard image processing tools. The reasons for this superiority is explained.

II. Image Formation Model

A. The Signal

As depicted in Fig. 1, under natural illumination we sense two sources. The first source is the scene object. The image of this source is degraded, as we detail below, and we term it as the *signal*. The second source is the ambient illumination. Part of the ambient light is scattered towards the camera by the particles in the water, and is termed *veiling light* or *backscattered light* [16][21]. The description of the latter component is given in Sec. II-B.

In the literature, the signal is typically represented as a sum of two components, termed *direct transmission* and *forward scattering* [16][21]. The direct transmission is given by

$$D(x,y) = L_{\text{object}}(x,y)e^{-\eta z} \quad , \tag{1}$$

where η is the attenuation coefficient, and z is the distance to the object. This distance depends on the pixel coordinates x and y. Here L_{object} is the object radiance we would have sensed, had there been no scattering and absorption along the line of sight (LOS).

The forward scattering component is similar to the direct transmission. However, it represents light scattered at small angles relative to the LOS, causing image blur. It has been expressed as

$$F(x,y) = D(x,y) * g_z(x,y) \quad , \tag{2}$$

where D is given by (1) and g_z is a point spread function (PSF). The PSF [16][21] is parameterized by the distance z, since the farther the object, the wider the support of the blur kernel.
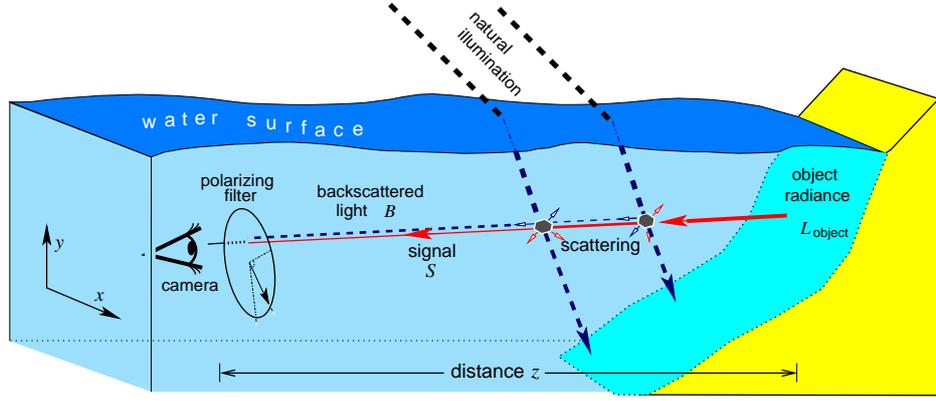
Fig. 1. [Dashed rays] Backscatter: Light coming from a source is scattered towards the camera by particles in the water. This component increases with the distance z to the object. [Solid ray] Signal: Light emanating from the object is attenuated and somewhat blurred as z increases. Without scattering and absorption along the line of sight (LOS), the object radiance would have been L_{object}.

Accounting for both the direct transmission (1) and the forward scattering (2), we define the *signal* as

$$S = D + F \; . \tag{3}$$

In addition, we define an *effective object radiance* $L_{\text{object}}^{\text{effective}}$ as

$$L_{\text{object}}^{\text{effective}} = L_{\text{object}} + L_{\text{object}} * g_z \; . \tag{4}$$

It is a somewhat blurred version of L_{object}. From (1,2,3), the signal is

$$S = e^{-\eta z} \, L_{\text{object}}^{\text{effective}} \; . \tag{5}$$

In [28] we demonstrated that blur due to forward scattering is generally not the dominating contributor to image degradation. Rather, image degradation occurs mainly due to the veiling light, described in Sec. II-B. For this reason, our recovery approach, described in Sec. III, does *not* attempt to compensate for image blur, say by deconvolution. Hence, we do not seek, at this point, to recover L_{object}, but make do with the recovery of $L_{\text{object}}^{\text{effective}}$ from the signal. For this reason, we prefer the signal representation of (5), rather than using the more familiar representation of (3).

B. Veiling Light

Veiling light is often referred to in the literature as *backscatter*. We thus use these terms interchangeably. It is caused by scattering the ambient illumination into the LOS and towards the camera by suspended particles (Fig. 1). Consider a single distant source that illuminates the LOS from direction $\vec{r} = (\theta, \varphi)$ relative to the LOS, with intensity I^{source}. Following [16][21], the contribution of this source to the backscatter is

$$B(\vec{r}) = \int_0^z \beta(\theta) \, I^{\text{source}}(\vec{r}) \, e^{-\eta l} \left[1 - \frac{f}{l + l_0} \right]^2 dl \tag{6}$$

where f is the focal length of the camera and l_0 is the distance between the lens and the underwater housing window. Here $\beta(\theta)$ is the angular scattering coefficient.

In [28] we have shown that (6) can be greatly simplified. Integrating the illumination distribution caused by distant light sources in all directions, the backscatter can be approximated by

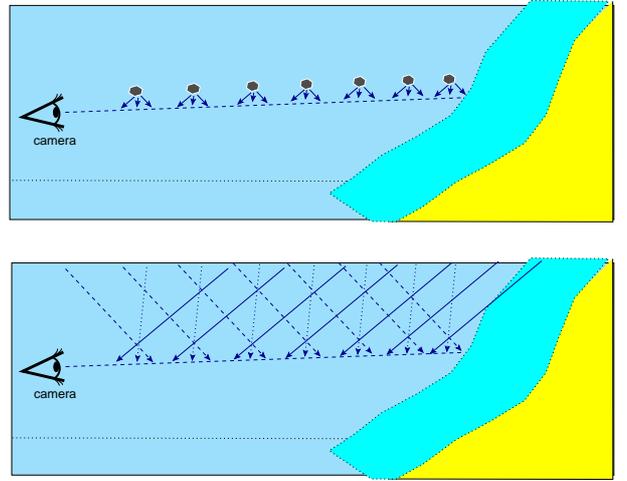$$B = B_\infty \left(1 - e^{-\eta z} \right) \; , \tag{7}$$

Fig. 2. [Top] Light from close sources. [Bottom] Light from non-distant sources can be represented as originating from equivalent sources at infinity.

where B_∞ is the backscatter in a LOS which extends to infinity in the water. This approximation is accurate to 99%, when accounting for the practical orders of magnitude of focal lengths vs. attenuation distances [28]. The constant B_∞ depends on the wavelength λ. In addition, the wavelength affects the values of η, g_z and β in (1,2,5-7).

Fig. 2 shows that light from the non-distant particles can be represented as originating from equivalent sources at infinity. This is based on an assumption of homogeneous lighting along the LOS. We believe that this is a reasonable assumption in horizontal photography. The reason is that underwater lighting naturally comes from a limited light cone directly *above* [15], and is thus typically unobscured along the LOS. Thanks to this equivalence, the expression (7) which was developed for distant light sources is applicable to the general case of non-distant light sources (as particles suspended in the water volume).

The total image irradiance is

$$I^{\text{total}} = S + B = e^{-\eta z} \, L_{\text{object}}^{\text{effective}} + B \; . \tag{8}$$

The veiling light thus acts as a bias which reduces the

detected contrast. In fact [28], this bias often overwhelms the attenuated signal.

A major problem stems from the spatial dependence of the degradation effects. Image pixels at various coordinates (x, y) correspond to objects at different distances z. As indicated in (5,7) and (8), the backscatter and the attenuation depend on z, and thus implicitly depend on the image coordinates x and y. The consequence of this aspect is that any attempt to invert the image formation process in order to recover the scene must be spatially varying, i.e., it must account for the range of distances in the scene. For this reason, standard image processing yield only a limited improvement, as we show in Sec. IV.

C. Polarization Effects

It has been known that various marine animals use polarization for improved vision [8][26][38][40]. This has encouraged researchers to find an analogous artificial method for improved computer vision. Before dealing with those past attempts and with our approach, we shall now briefly describe the related natural polarization effects.

Under natural illumination, the *veiling light is partially polarized horizontally* [7][15][38]. The reason is that off-axis scattering of light has different intensities for different polarization components. In particular, the strongest scattering occurs for the polarization component perpendicular to the plane formed by the LOS and the off-axis illumination ray. The weakest scattering occurs for the polarization component parallel to this plane. Since underwater lighting naturally comes from a limited light cone directly *above* [15] the LOS, the dominant polarization component is horizontal. These extrema of the backscatter (strongest and weakest scattering) correspond to values $B^{\max}$ and $B^{\min}$, where

$$B = B^{\max} + B^{\min} \tag{9}$$

is given by (7). The backscatter degree of polarization is defined as

$$p \equiv \frac{B^{\max} - B^{\min}}{B} \quad . \tag{10}$$

We assume that the polarization of the veiling light dominates the overall measured polarization, and neglect polarization associated with the signal S. This is an important aspect which distinguishes our work from most of the prior polarization-related methods. The reasons for this assumption are detailed in [28]. The validity of this assumption has recently been verified independently by [30].

III. Scene Recovery

To recover the scene, we first image it via a polarizing filter. We take two images, each using a different state of the polarizer. Similarly to backscattered light, there are two orthogonal polarizer angles corresponding to extrema of the intensity, $I^{\max}$ and $I^{\min}$, where

$$I^{\max} = S/2 + B^{\max} \quad \text{and} \quad I^{\min} = S/2 + B^{\min} \ . \tag{11}$$

In consistency with our assumption that the signal polarization is insignificant, the signal makes the same contribution

to both images, as expressed in (11). These are orthogonal polarization components, whose sum

$$I^{\text{total}} = I^{\max} + I^{\min} \tag{12}$$

is given by (8). Note that $I^{\min}$ is the image taken at the "best state" of the polarizer, where the disturbing backscatter is minimal [38].

These raw images become the input for the recovery algorithm. Assume for a moment that we have an estimate of the global parameters B_∞ and p. From (9,10,11), we estimate the veiling light as

$$\hat{B} = \frac{I^{\max} - I^{\min}}{p} \quad . \tag{13}$$

Inserting this estimate into (7,8,12), we recover the object radiance

$$\hat{L}_{\text{object}}^{\text{effective}} = \frac{I^{\text{total}} - \hat{B}}{\hat{t}} \quad , \tag{14}$$

where

$$\hat{t} = 1 - \frac{\hat{B}}{B_\infty} \ . \tag{15}$$

Here $\hat{t}$ is the estimated water transmittance, which is related to the object distance z by

$$\hat{t} = \exp(-\eta z) \ . \tag{16}$$

We process each color channel independently this way.

As mentioned above, we need estimates of the global parameters B_∞ and p. These are intrinsic parameters of the water and lighting. We obtain these estimates by measuring pixels corresponding to objects "at infinity", i.e., which are so distant inside the water, that their signals are negligible due to attenuation. The visibility range underwater is very short. Therefore, there are usually plenty of horizontal viewing directions in which no object is visible.

We should note that there are several additional details related to the method. These include regularization of the results and color correction. While they are not the core of the method, they are important for obtaining good results. The reader is thus directed to [28] for further details.

We have conducted several experiments in the sea, and obtained significant improvements. In the following, we concentrate on one of these experiments. Additional underwater experiments are shown in [27]. The raw images in Fig. 3 were taken at a depth of 26 meters in Eilat (the Red-Sea), during the day. The raw images have a very low contrast. The result of the full scene recovery algorithm is shown on the right part of Fig. 4. Compare this result to the left part of Fig. 4, in which a simple white-balancing operation was performed. The image recovered by our method has a much improved contrast and color. The recovered image shows details unseen in the input images, especially in areas corresponding to far objects.

IV. Comparison to Prior Passive Methods

A. Standard Image Processing

In this section we compare our results to prior methods that rely on natural illumination. Here we discuss standard image processing procedures. First, consider standard image sharpening, as obtained by the *unsharp masking* [18]
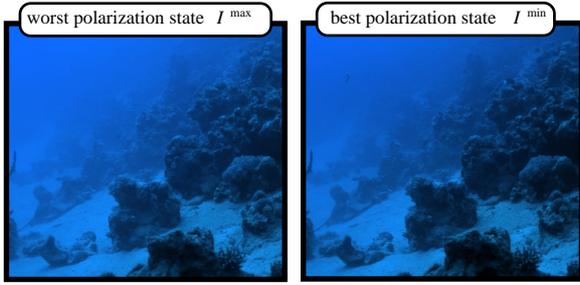
Fig. 3. Images were taken using horizontal and vertical polarizer orientations. Both color images are contrast stretched, yet their visibility is poor.
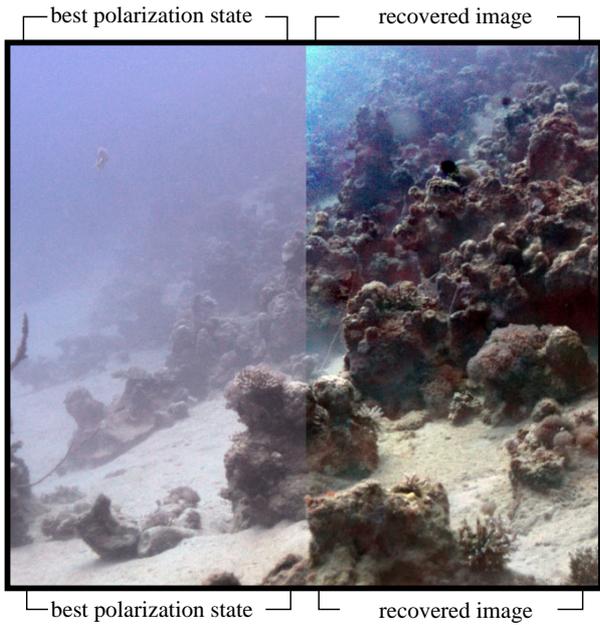

Fig. 4. [Left] A white-balanced version of the best raw image. The colors and visibility quickly degrade as objects become more distant. [Right] In the image recovered by our polarization-based method, image colors and contrast are recovered to large distances.

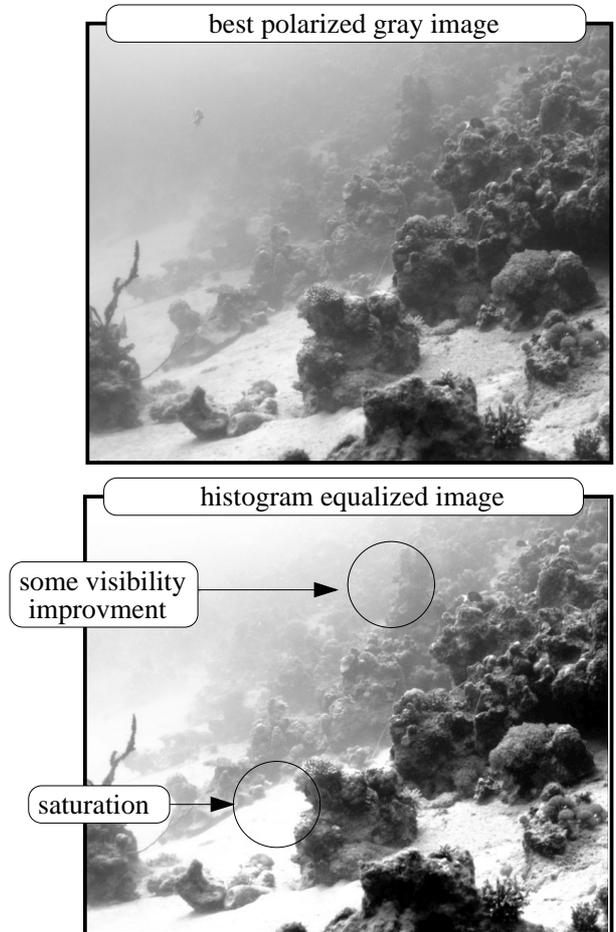Fig. 5. The sharpened image, without the recovery process.

Fig. 6. [Top] The image $I^{\min}$ in grayscale. [Bottom] The result of histogram equalization. While visibility has improved somewhat in areas corresponding to distant objects, it has become worse in areas corresponding to objects at close distance.

operation. The result of this method is shown in Fig. 5. This method sharpens the images, but only slightly improves the long-range visibility, relative to the unrecovered image shown on the left part of Fig. 4. A by-product (as typical in sharpening operations) is amplification of high frequency noise.

Next, consider the operation of histogram equalization. The result of this method is shown in Fig. 6. It slightly improved the areas corresponding to distant objects, but the visibility of close objects deteriorated due to saturation. Moreover, histogram equalization of color images is ill defined, and therefore colors are generally distorted by this operation. For this reason, we display the histogram-equalized image in grayscale. The method does not recover the proper relation between the different colors.

As previously described, underwater the contrast loss is strongly affected by the distance and is therefore spatially varying (in the image plane). However, most image processing methods (as histogram equalization and unsharp masking) are space invariant, and do not account for the distance dependencies. For this reason, the effectiveness of the standard image processing methods is limited.
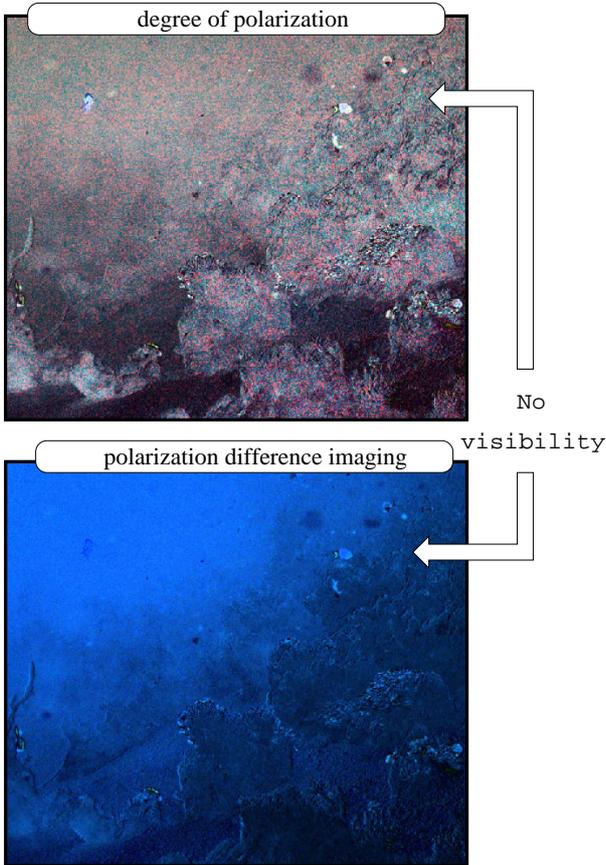
Fig. 7. Results of past methods for polarization-based enhancement. The DOP is displayed at the top, while the PDI is displayed on the bottom. Those results are not helpful for visibility recovery. In some places the visibility is ruined.

B. Polarization Difference

Some studies had suggested image analysis of polarization filtered images. Most of them have been based either on a simple subtraction of the raw images that are differently polarization filtered [13], or displaying [26][33] the degree of polarization (DOP) of the sensed light. The polarization difference image (PDI) is defined as

$$\mathrm{PDI} \equiv I^{\mathrm{max}} - I^{\mathrm{min}} \quad . \tag{17}$$

while the DOP of the detected light is

$$\mathrm{DOP} \equiv \frac{I^{\mathrm{max}} - I^{\mathrm{min}}}{I^{\mathrm{total}}} \quad . \tag{18}$$

Implicitly, those methods assume that polarization is associated with the object radiation (and thus the signal), rather than with the veiling light. This is in contrast to our assumptions, mentioned in Sec. II-C.

Fig. 7 shows the results of those methods, as applied to the raw data. These images indicate that those methods failed to recover the scene visibility, especially at long distances. It may even appear that the results are less comprehendible than the raw images.

The problem that undermines those methods is the assumption that signal polarization is significant. This assumption becomes invalid as distances increase [22], [30]. Thus, those methods become ineffective there.
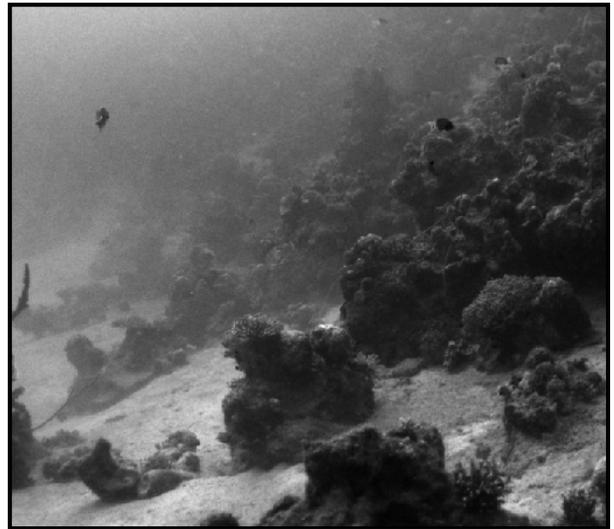

Fig. 8. Result of the method suggested by [5].

C. Polarization Association to Backscatter

Recently, an independent study [5] has also associated the polarization of light with underwater veiling light. However, that method is different from ours in the way the images are processed. Ref. [5] has an insight about the relation between polarization and backscatter, but the eventual image processing appears arbitrary. It is done by calculating a measure termed E, given by

$$E \equiv (m - \mathrm{DOP})\left(I^{\mathrm{total}} - n\right) \quad , \tag{19}$$

where the DOP was defined in (18). Here n is the intensity value of the dimmest image pixel, while m is the DOP of the most polarized image pixel.

When applied to the raw images we took in the ocean, the method of [5] yields the result given in Fig. 8. This image is in grayscale, because that method was not formulated for color. The result does not appear to recover a good visibility of the scene, particularly at long distances.

V. RECOVERING 3D STRUCTURE

The method we propose recovers the three dimensional structure of the scene. This is a major advantage, because none of the above mentioned methods has this capability. Based on (16), the distance z is estimated as a function of (x, y) up to a global scale factor η . It is given by

$$\widehat{\eta z}(x, y) = -\ln\left[1 - \frac{\hat{B}(x, y)}{B_\infty}\right] \quad . \tag{20}$$

If we know the distance to a single point, we can set the scale of the relative distance map.

The recovered range map can be used to render the scene from viewpoints other than the ones used during acquisition. We used the estimated range map to create a 3D surface, and changed the viewpoint. To emphasize the difference between the viewpoints, we inserted virtual objects into the scene (four colored spheres) as in Fig. 9.
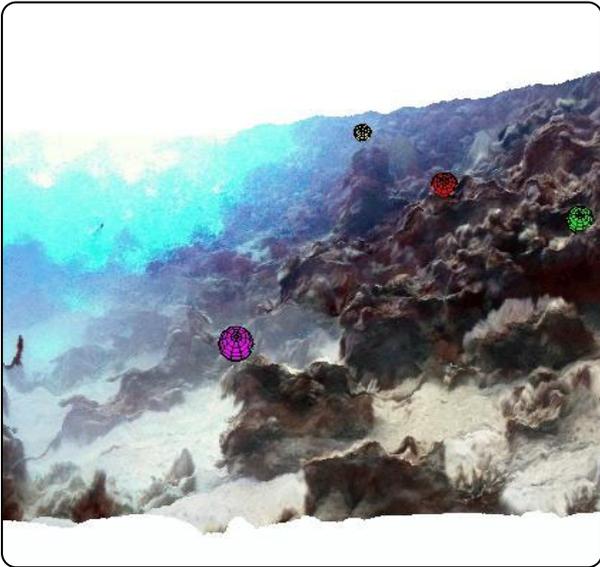
Fig. 9. We use the recovered 3d scene, to render an image showing the scene as if seen from a viewpoint different than the one used during acquisition. This novel image contains virtual objects (colored spheres) into the 3D scene, to illustrate occlusion effects.

VI. COMPARISON TO ACTIVE METHODS

To complete the description of the context of this approach, we now refer to active optical methods. In these methods, light is radiated into the scene by the system. They include optical time gating [13][14][19][32], time gated fluorescence [31], confocal illumination [20], and synchronous (stripe) scan [16][17][19]. Some of these active methods provide range information. Other methods rely on polarized light sources [11][13][36]. How does our method compete with those?

To begin with, we should state the current limitations of our method. The most obvious limitation is that it requires daylight. In addition, it is currently formulated for horizontal photography. The reason is that we assume homogenous illumination along the LOS, and we also assume polarization induced by this illumination. Both of these assumption are met when viewing horizontally, as the natural illumination irradiates the LOS from a favorable direction. In addition, the method assumes that hydrosols help in polarizing the veiling light, rather than depolarizing it. This may not always happen. The active optical methods mentioned above do not suffer from these limitations, and thus possess strong advantages.

Nevertheless, these active methods have shortcomings. Light has to go through the medium all the way to the object - and back. Therefore, the object irradiance decreases exponentially with distance due to attenuation, beyond the $1/z^2$ falloff of free space propagation. This limits the working range of active sensors. This problem often requires such systems to be highly power consuming, complex, and very expensive. In contrast, natural illumination, when available, exists all over the scene, alleviating much of this problem in our method.

In addition, some of the active sensors are based on

scanning, either strips or transversal planes. This scan may require a long time to complete, in contrast a method which is simply based on a couple of images taken through a polarizer.

VII. CONCLUSIONS

The method we presented is simple, both with respect to the acquisition hardware, and with respect to the image analysis algorithm. Thanks to its reliance on the physical models of image formation, it enables a very effective recovery of the scene, i.e., clear visibility and 3D structure. As discussed in Sec. VI, the current formulation is tailored to horizontal photography in daylight. Nevertheless, our plans are focused on extending the formulation to active illumination and oblique photography. Link to [27] for additional results and experiments.

REFERENCES

[1] L. Botelho-Ribeiro, "Underwater vision method for low-visibility turbulent conditions," *Proc. MTS/IEEE Oceans*, vol. 2, pp. 1080–1084, 2001.

[2] T. Boult, "DOVE: Dolphin omni-directional video equipment," *Proc. Int. Conf. Robotics & Autom.* pp. 214-220, 2000.

[3] M. J. Buckingham, J. R. Potter and C. L. Epifanio "Seeing underwater with background noise," *Scientific American* vol. 274/2, pp. 40-44, 1996.

[4] J. W. Caruthers, R. R. Goodman, M. A. Wilson and S. J. Stanic, "High-frequency acoustics seafloor scattering with emphasis on development of a new side-scan sonar," *Proc. IEEE Oceans*, vol. I, pp. 363-368, 2002.

[5] P. C. Y. Chang, J. C. Flitton, K.I. Hopcraft, E. Jakeman D. L. Jordan and J. G. Walker, "Improving visibility depth in passive underwater imaging by use of polarization,", *App. Opt.* vol. 42 pp. 2794-802, 2003.

[6] D. F. Coleman, J. B. Newman, and R. D. Ballard, "Design and implementation of advanced underwater imaging systems for deep sea marine archaeological surveys," *Proc. MTS/IEEE Oceans*, vol. 1, pp. 661–665, 2000.

[7] T. W. Cronin and N. Shashar, "The linearly polarized field in clear, tropical marine waters: spatial and temporal variation of light intensity, degree or polarization and e-vector angle," *J. Experim. Biol.*, vol. 204, pp. 2461-2467, 2001.

[8] T. W. Cronin, N. Shashar, R. L. Caldwell, J. Marshall, A. G. Cheroske and T. H. Chiou "Polarization vision and its role in biological signalling," *Integrative & Comperative Biol.* vol. 43, pp. 549-558, 2003.

[9] J. L. Forand, G. R. Fournier, D. Bonnier, and P. Pace, "LUCIE: a laser underwater camera image enhancer," *Proc. IEEE OCEANS*, vol. 3, pp. 187–190, 1993.

[10] G. L. Foresti, "Visual inspection of sea bottom structures by an autonomous underwater vehicle," *IEEE Trans. Syst. Man and Cyber, Part B*, vol. 31, pp. 691-705, 2001.

[11] G. D. Gilbert and J. C. Pernicka, "Improvement of underwater visibility by reduction of backscatter with a circular polarization technique," *App. Opt.*, vol. 6, pp. 741–746, 1967.

[12] S. A. L. Glegg, M. P. Olivieri, R. K. Coulson and S. M. Smith, "A passive sonar system based on an autonomous underwater vehicle," *IEEE J. Oceanic Eng.*, vol. 26, pp. 700-710, 2001.

[13] S. Harsdorf, R. Reuter and S. Tönebön, "Contrast-enhanced optical imaging of submersible targets," *Proc. SPIE*, vol. 3821, pp. 378-383, 1999.

[14] Duo-Min He and G. G. L. Seet, "Divergent-beam lidar imaging in turbid water," *Optics and Lasers in Engineering*, vol. 41, pp. 217-231, 2004.

[15] G. Horváth and C. Varjú, "Underwater refraction-polarization patterns of skylight percieved by aquatic animals through Snell's window of the flat water surface," *Vision Research*, vol. 35, pp. 1651-1666, 1995.

[16] J. S. Jaffe, "Computer modeling and the design of optimal underwater imaging systems," *IEEE J. Oceanic Eng.*, vol. 15, pp. 101-111, 1990.

[17] J. S. Jaffe, "Sensors for underwater robotic vision: status and prospects," *Proc. IEEE Int. Conf. Robotics and Automation,* pp. 2759-2766, 1991.

[18] A. K. Jain, *Fundamentals of digital image processing.* Prentice-Hall, 1989.

[19] D. M. Kocak and F. M. Caimi, "Computer vision in ocean engineering," *The Ocean Eng. Handbook*, editor F. El-Hawari, Ch. 4.3, CRC Press, 2001.

[20] M. Levoy, B. Chen, V. Vaish, M. Horowitz, I. Mc-Dowall and M. Bolas, "Synthetic aperture confocal imaging," *Proc. SIGGRAPH*, 2004.

[21] B. L. McGlamery, "A computer model for underwater camera system," *Proc. SPIE* vol. 208, pp. 221-231, 1979.

[22] S. P. Morgan, M. P. Khong and M. G. Somekh "Effects of polarization state and scatterer concentration on optical imaging through scattering media," *App. Opt.*, vol. 36, pp. 1560-1565, 1997.

[23] A. Ortiz, M. Simo and G. Oliver, "A vision system for an underwater cable tracker," *Machine Vis. and App.*, vol. 13, pp. 129-140, 2002.

[24] Y. Petillot, I. Tena Ruiz, D. M. Lane, Y. Wang, E. Trucco and N. Pican "Underwater vehicle path planning using a multi-beam forward looking sonar" *Proc. IEEE Oceans*, Vol. II, pp. 1194-1199 1998.

[25] J. Potter and M. Chitre "Ambient noise imaging in warm shallow seas; second order moment and model-based imaging algorithm" *J. Acoust. Soc. Amer.*, vol. 106/6, pp. 3201-3210, 1999.

[26] M. P. Rowe, E. N. Pugh Jr., J. S. Tyo, and N. Engheta, "Polarization-difference imaging: a biologically inspired technique for observation through scattering media," *Optics Lett.*, vol. 20, pp .608-610, 1995.

[27] Y. Y. Schechner, *Home page*. Follow the links from http://www.ee.technion.ac.il/∼ yoav/

[28] Y. Y. Schechner and N. Karpel "Clear underwater vision," *Proc. IEEE Computer Vision and Pattern Recognition*, Vol. I, pp. 536-543, 2004.

[29] Y. Y. Schechner, J. Shamir and N. Kiryati, "Polarization and statistical analysis of scenes containing a semi-reflector," *J. Opt. Soc. Amer. A*, vol. 17, pp. 276-284, 2000.

[30] N. Shashar, S. Sabbah and T. W. Cronin, "Transmission of linearly polarized light in sea water: Implications for polarization signaling," *J. Experimental Biology*, vol. 207, 2004.

[31] D. N. Sitter Jr. and A. Gelbart, "Laser-induced fluorescence imaging of the ocean bottom," *Opt. Eng.*, vol. 40, pp. 1545-1553, 2001.

[32] B. A. Swartz, "Laser range gate underwater imaging advances," in *Proc. MTS/IEEE Oceans*, pp. 722–727, 1994.

[33] J. S. Talyor, Jr., and L. B. Wolff "Partial polarization signature results from the field testing of the SHallow water Real-time IMaging Polarimeter (SHRIMP)," *MTS/IEEE Oceans*, vol. 1, pp. 107-116, 2001, .

[34] P. Venugopalan, P. Deshpande, S. Badiu, S. Constantin, B. Lu and J. R. Potter, "A 1.6 gigabit/second, 25-85 kHz acoustic imaging array - novel mechanical and electronics design aspects," *Proc. IEEE/MTS Oceans*, vol. I, pp. 352-358, 1999.

[35] H. T. Vosbein, "Towards better sonar performance predictions," *Proc. IEEE Oceans*, vol. I, pp. 352-357, 2002.

[36] J. G. Walker, P. C. Y. Chang and K. I. Hopcraft, "Visibility depth improvement in active polarization imaging in scattering media," *App. Opt.*, vol. 39, pp. 4933-4941, 2000.

[37] D. Walther, D. R. Edgington and C. Koch, "Detection and tracking of objects in underwater video," *Proc. IEEE Int. Conf. Computer Vision*, vol. 1, pp. 544-549, 2004.

[38] R. Wehner, "Polarization vision - a uniform sensory capacity?" *J. Exp. Biol*, vol. 204, pp. 2589-2596, 2001.

[39] T. E. Wilcox and B. Fletcher, "High frequency side scan sonar for target reacquisition and identification," *Proc. IEEE Oceans*, vol. 4, pp. 1882-1887, 2003.

[40] L. B. Wolff, "Polarization vision: a new sensory approach to image understanding," *Image & Vision Comp.*, vol. 15, pp. 81-93, 1997.

[41] X. Xu and S. Negahdaripour, "Automatic optical station keeping and navigation of an ROV: sea trial experiment," *Proc. Oceans*, vol.1, pp. 71-76, 1999.